Return to Session Directory

DYNAMIC POSITIONING CONFERENCE
October 12-13, 2010

Thrusters

Comparison of Thruster Axis Tilting versus Nozzle Tilting on the Propeller-Hull Interactions for a Drillship at DP-Conditions

Michael Palm, Dirk Jürgens, David Bendl
Voith Turbo Marine, Heidenheim, Germany

1. INTRODUCTION

Azimuth-steerable thrusters are widely used in the offshore industry for efficient dynamic positioning. Due to the thruster-hull and thruster-thruster interactions the installed propulsion system may experience severe efficiency losses at DP conditions.

To provide a better understanding of these phenomena the authors presented a study on the interaction effects for a semi-submersible drill rig at the Dynamic Positioning Conference 2008.[1] It was shown that for such a twin hull configuration an inclined rotational axis can to a large extend reduce the thrust losses. In Fig. 1 the pressure distribution on the second pontoon illustrates the differences in interaction losses due to different thruster inclinations.

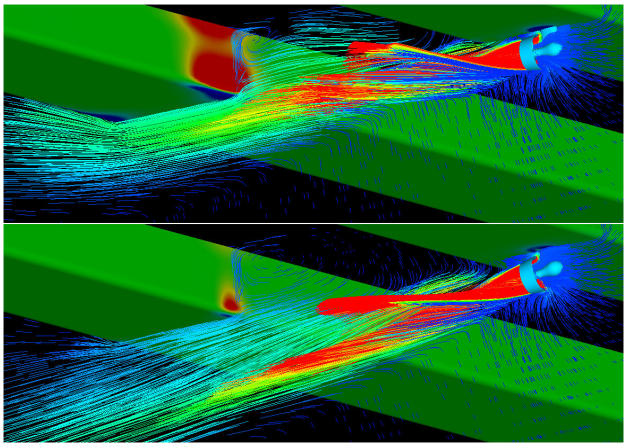

Fig. 1: Static pressure on second pontoon for 0° (top) and 8° axis tilt (bottom) on a twin hull configuration

In the current paper a CFD study is presented with the focus on a monohull vessel in order to detect possible benefits through axis tilting for this kind of ship class. Different thruster arrangements on a drill ship have been analysed to quantify the influence of thruster tilting with regard to interaction losses. The results for thrusters with gear-tilting are compared with a thruster that incorporates a horizontal propeller-axis and a tilted nozzle only.

The next section introduces briefly the solution method used. This is followed by sections describing the thruster and hull geometry and presenting the results of the CFD study. The final section summarizes the findings.

2. COMPUTATIONAL METHOD

All computations reported here are performed using the CFD software Comet. It is based on a finite-volume (FV) method and starts from conservation equations in integral form. With appropriate initial and boundary conditions and by means of a number of discrete approximations, an algebraic equation system solvable on a computer is obtained. First, the spatial solution domain is subdivided into a finite number of contiguous control volumes (CVs) which can be of an arbitrary polyhedral shape and are typically made smaller in regions of rapid variation of flow variables. The time interval of interest is also subdivided into time steps of appropriate size (not necessarily constant). The governing equations contain surface and volume integrals, as well as time and space derivatives. These are then approximated for each CV and time level using suitable approximations.

The flow is assumed to be governed by the Reynolds-averaged Navier-Stokes equations, in which turbulence effects are included via an eddy-viscosity model (k-ε or k-ω models are typically used). Thus, the continuity equation, three momentum component equations, and two equations for turbulence properties are solved. In addition, the space-conservation law must be satisfied because the CVs have to move and change their shape and location as the propeller starts to rotate. These equations are:

Mass conservation:

$$\frac{\mathrm{d}}{\mathrm{d}t}\int_V \rho \,\mathrm{d}V + \int_S \rho(\mathbf{v}-\mathbf{v}_\mathrm{b})\cdot\mathbf{n}\,\mathrm{d}S = 0$$

Momentum conservation:

$$\frac{\mathrm{d}}{\mathrm{d}t}\int_V \rho\mathbf{v}\,\mathrm{d}V + \int_S \rho\mathbf{v}(\mathbf{v}-\mathbf{v}_\mathrm{b})\cdot\mathbf{n}\,\mathrm{d}S = \int_S (\mathbf{T}-p\mathbf{I})\cdot\mathbf{n}\,\mathrm{d}S + \int_V \rho\mathbf{b}\,\mathrm{d}V$$

Generic transport equation for scalar quantities:

$$\frac{\mathrm{d}}{\mathrm{d}t}\int_V \rho\phi\,\mathrm{d}V + \int_S \rho\phi(\mathbf{v}-\mathbf{v}_\mathrm{b})\cdot\mathbf{n}\,\mathrm{d}S = \int_S \Gamma\nabla\phi\cdot\mathbf{n}\,\mathrm{d}S + \int_V \rho b_\phi\,\mathrm{d}V$$

Space-conservation law:

$$\frac{\mathrm{d}}{\mathrm{d}t}\int_V \mathrm{d}V - \int_S \mathbf{v}_\mathrm{b}\cdot\mathbf{n}\,\mathrm{d}S = 0$$

In these equations, ρ stands for fluid density, $\mathbf{v}$ is the fluid velocity vector and $\mathbf{v}_\mathrm{b}$ is the velocity of CV surface; $\mathbf{n}$ is the unit vector normal to CV surface whose area is S and volume V. $\mathbf{T}$ stands for the stress tensor (expressed in terms of velocity gradients and eddy viscosity), p is the pressure, $\mathbf{I}$ is the unit tensor, ϕ stands for the scalar variable (k or ε or ω), Γ is the diffusivity coefficient, $\mathbf{b}$ is the vector of body forces per unit mass and b_ϕ represents sources or sinks of ϕ. Since the CV can move arbitrarily, velocity relative to CV surface appears in the convective flux terms, and the time derivative expresses the temporal change along the CV-path.

It is beyond the scope of this paper to go into all the details of the numerical solution method, so only a brief description is given here; details can be found in [2].

All integrals are approximated by midpoint rule, i.e. the value of the function to be integrated is first evaluated at the centre of the integration domain (CV face centres for surface integrals, CV centre for volume integrals, time level for time integrals) and then multiplied by the integration range (face area, cell volume, or time step). These approximations are of second-order accuracy,

irrespective of the shape of the integration region (arbitrary polygons for surface integrals, arbitrary polyhedra for volume integrals). Since variable values are computed at CV centres, interpolation has to be used to compute values at face centres and linear interpolation is predominantly used. However, first-order upwind interpolation is sometimes blended with linear interpolation for stability reasons. In order to compute diffusive fluxes, gradients are also needed at cell faces, while some source terms in equations for turbulence quantities require gradients at CV centres. These are also computed from linear shape functions.

The solution of the Navier-Stokes equations is found by using a segregated iterative method, in which the linearised momentum component equations are solved first using prevailing pressure and mass fluxes through cell faces (inner iterations), followed by solving the pressure-correction equation derived from the continuity equation (SIMPLE-algorithm; see [2] for more details). Thereafter equations for volume fraction and turbulence quantities are solved; the sequence is repeated (outer iterations) until all non-linear and coupled equations are satisfied within a prescribed tolerance, after which the process advances to the next time level.

3. THRUSTER DESIGN

The thruster used in the current study is a Voith Radial Propeller (VRP) with an input power of 5500kW and a propeller diameter of 4.2m (Fig.2). This unit is equipped with a 98° bevel gear to implement the inclined rotational axis.
For comparison reasons all thruster arrangements on the drill ship have been simulated with the VRP at an 8° axis tilt and a rectangular radial propeller (RRP) with a horizontal rotational axis and nozzle inclination of 5°. All other geometrical features of the thruster have been left identical. Fig.3 shows both thruster configurations that have been used. The simulations were carried out at full scale.
The different nozzle and axis orientation lead to different performance characteristics. By adjusting the number of revolutions it was ensured, that both propellers generate the same amount of thrust.

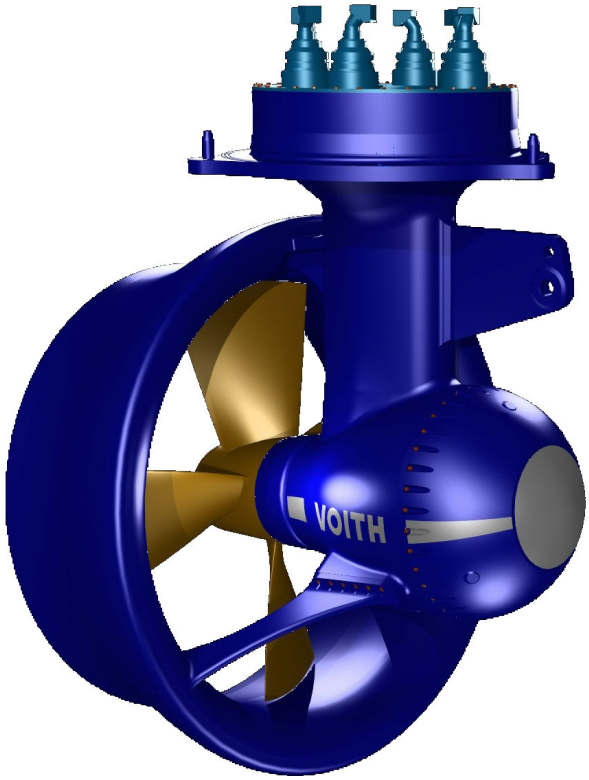

Fig. 2: Voith Radial Propeller 42-55

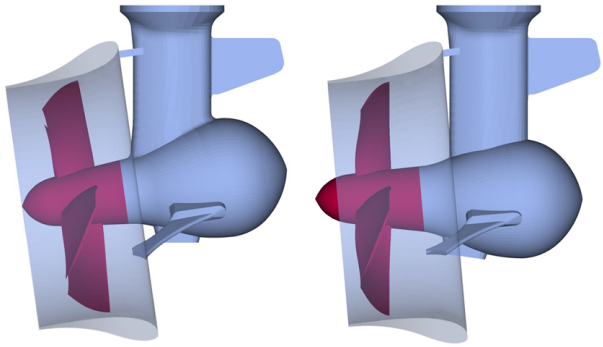

Fig. 3: VRP with 8° axis tilt (left) and RRP with 5° nozzle tilt (right)

4. INTERACTION LOSSES AT A SIMPLIFIED HULL SECTION

As a first step, the whole calculation setup was tested for plausibility at a simplified hull section with thrusters generating a transverse force. Fig. 4 shows the velocity field near the thruster and the resulting pressure distribution on the hull. As can be seen, the wake of the propeller interacts more pronouncedly with the hull in the RRP case. All computations have been carried out with a still standing vessel and an inflow velocity of zero.

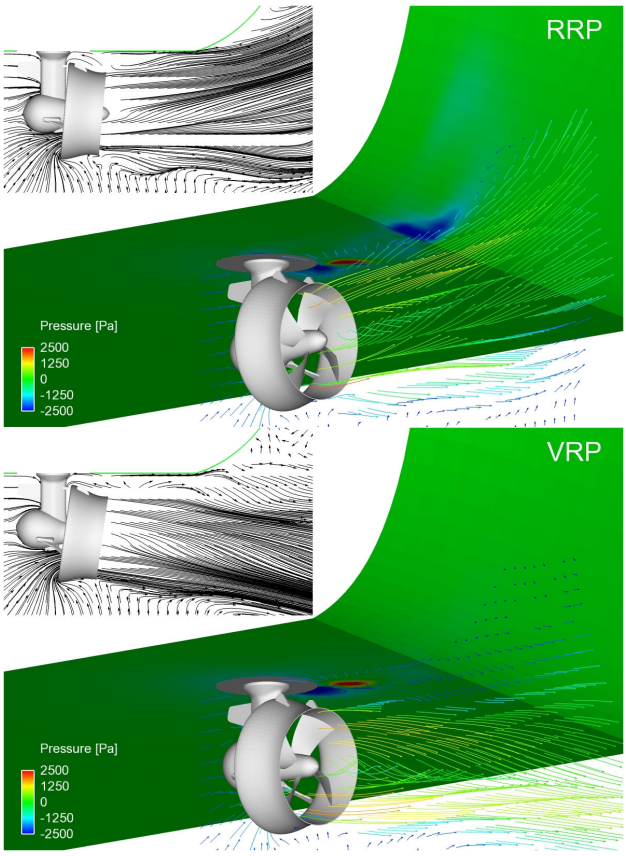

Fig. 4: pressure distribution on a hull section for the RRP (top) and VRP (bottom)

This is reflected through the region of lower static pressure in the area of the bilge radius.
This low pressure induces a force that opposes the nominal thrust direction of the propeller. As a result the effective thrust, which is meant to be the available force on the system hull-propeller, is decreased for the RRP.
While the thrust losses for the VRP amount to 1.2% they increase for the RRP to 4.2%.

5. DRILL SHIP DESIGN

The ship hull for this study was designed by Ulstein Sea of Solutions (Fig.5). The vessel has a length of 208m and a breadth of 32.2m. At an displacement of 42800t the draft amounts to 10.5m. The ship is equipped with six thrusters, three in the stern and three retractable types in the fore part.

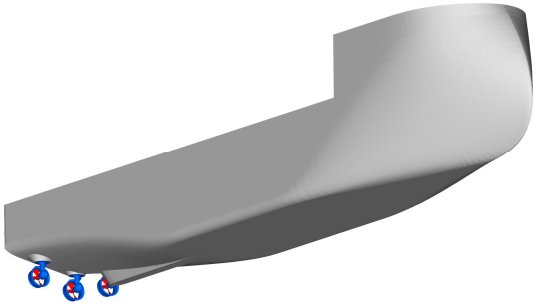

Fig. 5: hull lines by courtesy of Ulstein Sea of Solutions

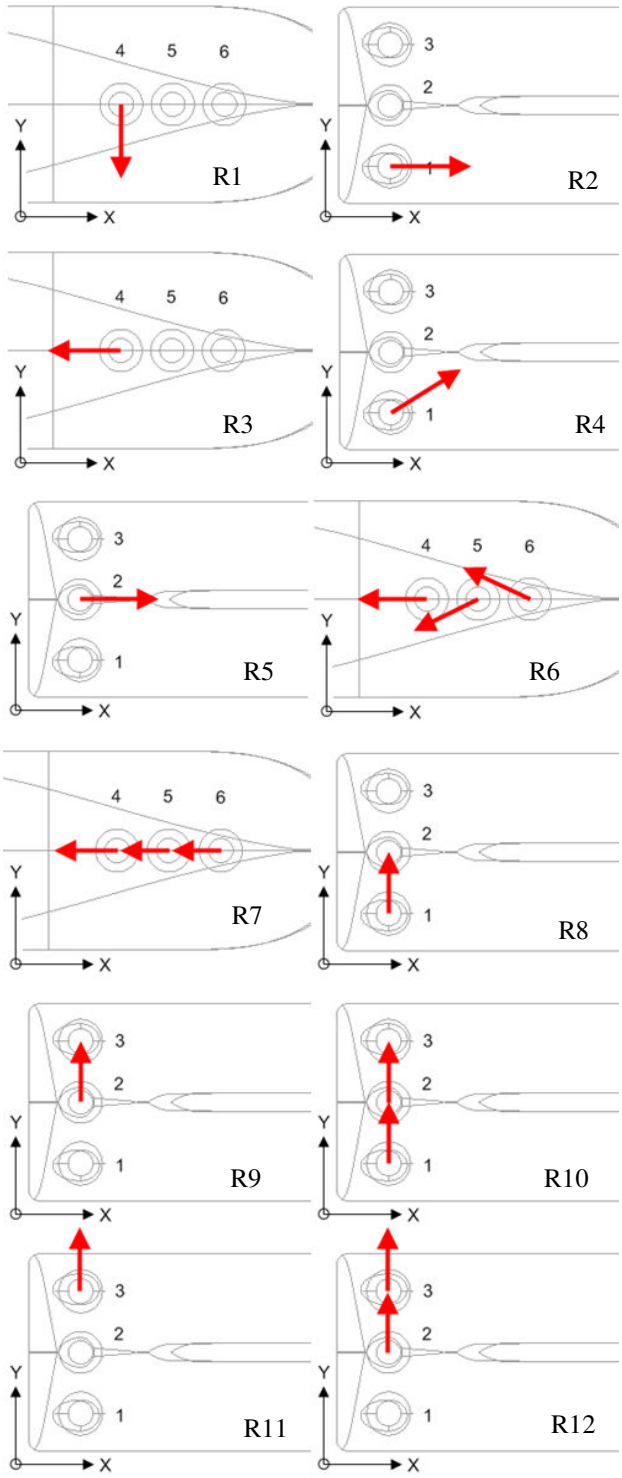

Fig. 6: investigated thruster configurations (arrows indicate wake direction)

In this study twelve different thruster arrangements were simulated. Fig.6 shows all configurations with the red arrows indicating the direction of the propeller wake. Although some thruster arrangements might be of academic nature due to lack of practical implementation, they have been investigated to cover a systematic range of different thruster-hull and thruster-thruster interaction incidents.

6. RESULTS

In the following section the results for all thruster configurations are presented and visualised for some selected cases. The denoted effective thrust for each configuration is defined as the total force acting on the system hull-thruster divided by the thrust of the propellers in each corresponding arrangement.
In the top part of Fig.7 the velocity field for arrangement R2 is shown, where the thrust is acting in sternwise direction. From the streamlines it can be concluded that the deflection ability of the inclined nozzle is somewhat limited compared to a fully inclined rotor axis.
The hull pressure in the lower part of Fig.7 indicates the unfavourable interactions which lead to an effective thrust of 91.8% for the RRP while the corresponding value for the VRP amounts to 96.1%.

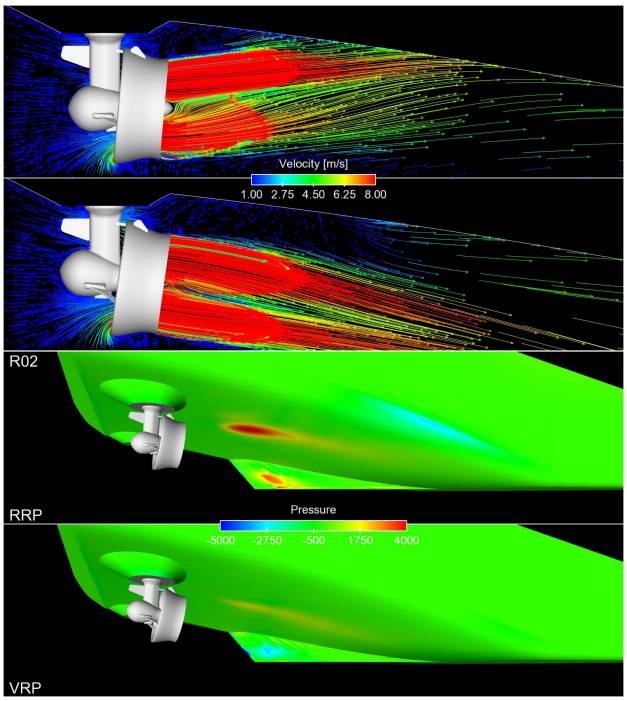

Fig. 7: velocity and pressure distribution for configuration R2 (RRP top, VRP bottom)

In case R6 the three bow thrusters are in focus. The two units near the bow have an azimuth angle of 35° towards the ships longitudinal axis.
The pressure distribution on the thrusters is depicted in Fig.8. In Fig.9 the velocity field illustrates the thruster-thruster interactions in this arrangement. In this case the effective thrust drops for the VRP to 89.6% and for the RRP to 83.8%. Due to the above-mentioned definition of the effective thrust, these values represent the losses due to hull-thruster interaction. An estimation of the thruster-thruster losses can be derived by comparison with configuration R3. Here the threefold thrust is approx. 22% higher than in R6. Comparing R6 with R7 the calculations show a thrust decrease for in-line arrangement in configuration R7 of approx. 37%.

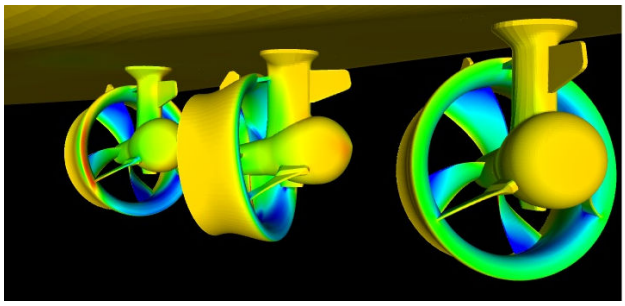

Fig. 8: velocity and pressure distribution for configuration R6

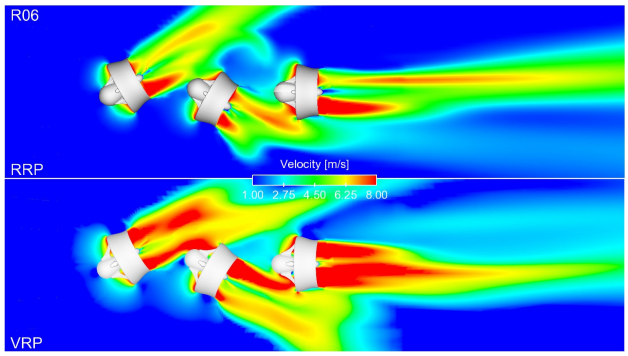

Fig. 9: velocity distribution for configuration R6

A configuration R8 that represents transverse thrust with the stern propellers is shown in Fig.10. Again an inclination of the rotor axis seems to be beneficial compared to a tilting of the nozzle only. The effective thrust decreases here to 76.8% for the VRP and to 60.7% for the RRP.

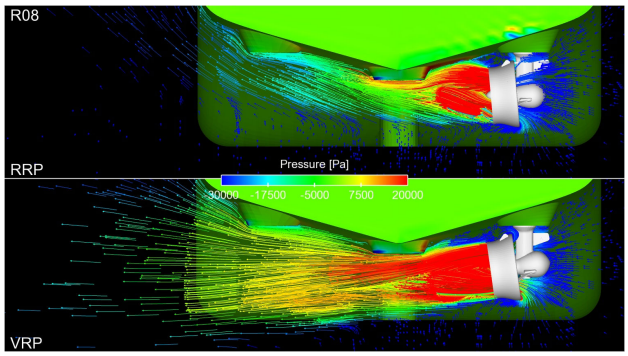

Fig. 10: velocity distribution for configuration R8

Activating also the centre thruster in addition to the starboard propeller leads to configuration R10. See Fig.11 for the velocity field. Here the effective thrust differences are of a similar magnitude compared to R8 giving a value of 89.0% for the VRP and 76.4% for the RRP.
Compared to the symmetrical arrangement of R12 where the port and the centre thruster are active (Fig.12), variant R10 produces 22% less thrust due to higher thruster-thruster losses. For R12, the effective thrust remains at a relatively high level of 94.8% for the VRP and 96.0% for the RRP evaluating the hull-thruster losses. Regarding the thruster-thruster losses, the variant

R12 generates 9% less thrust than the double value from configuration R9.

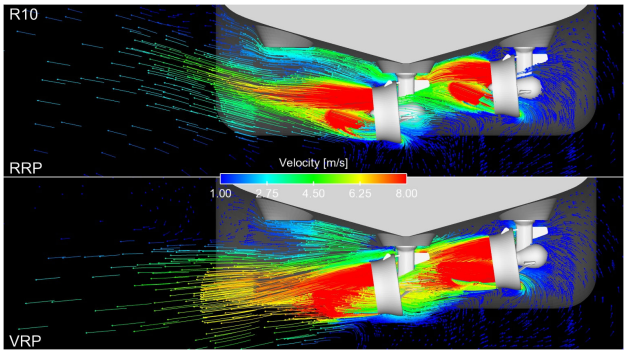

Fig. 11: velocity distribution for configuration R10

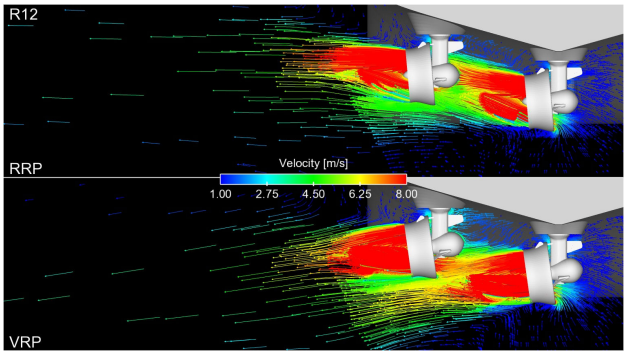

Fig. 12: velocity distribution for configuration R12

An overview on all investigated thruster arrangements is shown in Fig.13. The dark bars represent the effective thrust values for the VRP with 8° inclination while the bright bars indicate the corresponding values for the RRP with 5° nozzle tilt only.

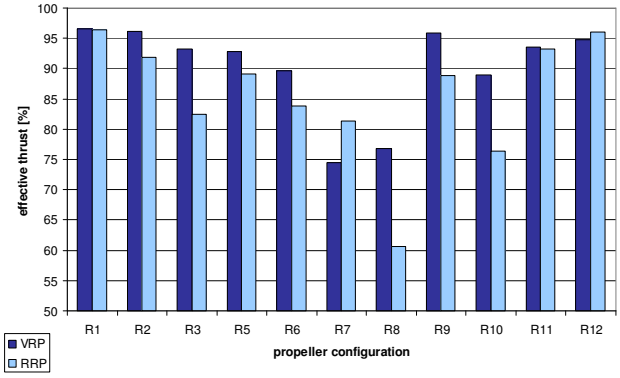

Fig. 13: effective thrust for different thruster arrangements

Configuration R4 was omitted from the diagram. Here the hull interaction led to very large hull forces that are directed almost perpendicular to the wake direction and therefore do not fit properly with the representation of the residual configurations. Fig.14 shows the flow pattern that makes the skeg act as a hydrofoil producing considerable lift forces.

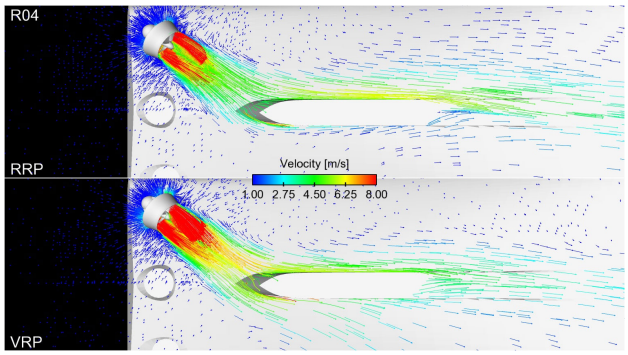

Fig. 14: velocity distribution for configuration R4

7. CONCLUSIONS

Except for variant R7, which corresponds to the in-line arrangement of the three bow thrusters and is avoided in practice anyhow, and variant R12 with only minor differences, all configurations have shown less thruster-hull or thruster-thruster interaction losses incorporating a 8° axis tilt.
As a result of the investigation, it can be concluded that tilting the axis by gear-tilt also offers advantages regarding the interaction effects for a monohull vessel.

8. REFERENCES

[1] D. Jürgens, M. Palm, A. Amelang, T. Moltrecht:
Design of Reliable Steerable Thrusters by Enhanced Numerical Methods and Full Scale Optimization of Thruster –Hull Interaction Using CFD
Dynamic Positioning Conference, Houston, 2008

[2] J. H. Ferziger, M. Perić:
Computational Methods for Fluid Dynamics
3rd ed., Springer, Berlin, 2003